International Journal of Thermophysics (2021) 42:57
https://doi.org/10.1007/s10765-021-02812-1

NANOPARTICLE-ENHANCED IONIC LIQUIDS

CFD Simulation of CO_2 Capture in a Microchannel by Aqueous Mixtures of MEA and [Bmim]BF_4 Modified with TiO_2 Nanoparticles

M. A. Makarem[1] · M. R. Kiani[2] · M. Farsi[1] · M. R. Rahimpour[1]

Received: 23 December 2020 / Accepted: 4 February 2021 / Published online: 26 February 2021

Abstract

In this research, a novel aqueous solvent, i.e., nanoparticle-enhanced ionic liquid (NEIL), is proposed for CO_2 capture by mixing of MEA as the base fluid and [Bmim]BF_4 ionic liquid and TiO_2 nanoparticles as chemical additives. Then, the flow hydrodynamics, mass transfer characteristics, and CO_2 absorption performance of the proposed solvent are investigated in a T-shaped microchannel structure by Computational Fluid Dynamics technique at steady-state condition. To present a detailed model, the Navier–Stokes and continuity equations are combined with a two-phase laminar flow module considering mass transfer between heterogeneous phases. Then, the effects of [Bmim]BF_4 and TiO_2 mass fraction on CO_2 loading, bubble formation, and velocity profile are investigated at different gas and liquid holdups at ionic liquid fraction 0 % to 10% and nanoparticle fraction 0 to 0.1%. It concludes that the purification fraction reaches a maximum at TiO_2 weight fraction 0.04% and applying solvent with high nanoparticle content decreases purification fraction. In general, the proposed solvent and the considered contactor present adequate performance to absorb CO_2 from the gas mixture.

Keywords Carbon dioxide capture · CFD simulation · Ionic liquid · Microchannel · Nanofluid

Nomenclature

a	Interfacial area (m^2)
c	Concentration ($mol \cdot m^{-3}$)

This article is part of the Special Issue on Nanoparticle-enhanced Ionic Liquids.

✉ M. Farsi
farsi@shirazu.ac.ir

✉ M. R. Rahimpour
rahimpor@shirazu.ac.ir

[1] Department of Chemical Engineering, Shiraz University, Shiraz, Iran

[2] College of Engineering, Fouman Faculty of Engineering, University of Tehran, Fouman, Iran

D	Diffusion coefficient ($m^2 \cdot s^{-1}$)
d	Nanoparticle diameter
E	Enhancement factor
F	Volume force vector ($N \cdot m^{-3}$)
H	Henry's constant ($Pa \cdot m^3 \cdot mol^{-1}$)
I	Gas–liquid interface
ILs	Ionic liquids
k	Reaction rate constant
k_L	Liquid side mass transfer coefficient ($m \cdot s^{-1}$)
n	Normal vector
p	Pressure (Pa)
R	Total mass transfer rate expression ($mol \cdot m^{-3} \cdot s^{-1}$)
Re	Reynolds number
S	Strain rate tensor
Sc	Schmitt number
t	Time (s)
u	Velocity vector ($m \cdot s^{-1}$)
w	Mass fraction
x	Channel length (m)

Greek Letters

μ	Dynamic viscosity ($Pa \cdot s^{-1}$)
γ	Reinitialization parameter ($m \cdot s^{-1}$)
ε	Interface controlling parameter (m)
ϕ	Volume fraction
φ	Volume concentration of nanoparticle
τ_c	Residence time (s)
τ_f	Viscous stress tensor (Pa)
ρ	Density ($kg \cdot m^{-3}$)
η	Purification fraction

Abbreviations

AMP	Aminomethyl propanol
DEA	Diethanolamine
MDEA	Methyl diethanolamine
MEA	Monoethanolamine
NEILs	Nanoparticle-Enhanced Ionic liquids
NPs	Nanoparticles
$[Bmim]BF_4$	1-Butyl-3-methylimidazolium tetrafluoroborate

1 Introduction

Recently, the emission of a large amount of CO_2 as a greenhouse gas into the atmosphere has caused climate change and global warming in the world. The exhaust stream from power plants and industrials such as steel, cement, chemicals, oil, and

gas refineries increases the concentration of carbon dioxide in the atmosphere and causes global warming. Typically, flooding in coastal cities, sequential droughts, devastating hurricanes, food and water shortages, and the prevalence of communicable diseases are just some consequences of worldwide warming.

Between the developed technologies for CO_2 capture, the absorption by alkanolamines including MEA, DEA, AMP, and MDEA is more popular and widely used in industrial plants. Since the common apparatus used in absorption processes have low efficiency, different improving methods have been proposed to enhance absorption efficiency such as applying novel solvents and increasing mass transfer coefficient by employing microchannels. In the recent decade, ionic liquids have been introduced as potential candidates for CO_2 absorption, due to the particular functional groups and unique molecular structures which lead to unique absorption properties [1]. These unique properties include but are not limited to high selectivity, loading, designability, non-volatility, and thermal stability [2, 3]. Particularly, the absorbed CO_2 can be easily regenerated from the saturated solvent, and applying ILs in the absorption process leads to a reduction in energy consumption and environmental concerns compared to conventional amine blends [4]. In addition, the use of ILs in the CO_2 absorption process instead of traditional volatile solvents can avoid solvent loss into the purge gas and reduces contaminant emission into the atmosphere [5]. Moreover, the structure tunability makes ionic liquids chemically designable with special characteristics for cost-effective and energy-efficient CO_2 absorption [5–7]. The conducted researches proved that adding ILs to conventional alkanolamines can improve the CO_2 absorption rate and loading. ILs can physically absorb CO_2 and improve the CO_2 absorption of conventional solvents [8]. In addition to enhancement in heat transfer characteristics [9], nanofluids are other modifiers that could improve the CO_2 absorption and enhance the mass transfer rate further [10]. Based on the conducted researches, the enhancement factor is improved up to 1.22 in TiO_2 nanoparticle-modified solvents, which means 22 % more enhancement in the mass transfer rate [11]. Integration of nanotechnology and thermophysical properties of ILs can develop a newly improved type of solvents entitled nanoparticle-enhanced ionic liquids (NEILs). Due to the good heat transfer properties and thermal stability of NEILs, these solvents are attractive in the heat transfer field [12, 13]. However, modification of the mixture of conventional alkanolamines and ILs with nanoparticles could improve the CO_2 absorption extremely.

Although substitution or mixing of conventional solvents with ILs and nanofluids could enhance absorption efficiency, the contractors are one of the main controlling parts that limit the process performance. Applying rotating packed beds and microchannels in gas purification units could enhance the mass transfer rate between phases and CO_2 absorption rate when mass transfer resistance is the controlling step [14, 15]. The conventional contactors such as packed beds and tray columns usually suffer from low gas–liquid interfacial area [16]. Recently, owing to the advantages of micro-dispersion systems such as providing large contact area, controllability, safety, high mass transfer rate, and repeatability, this type of system was suggested for absorption processes [17]. Because of high phase dispersion in the micro-scale structures, both mass and heat transfer can be extremely enhanced simultaneously [18–21]. In comparison with the conventional apparatus, microchannels can enhance the mass transfer coefficient up to

1000 times [22]. Guo et al. experimentally investigated CO_2 absorption in a T-junction microchannel and found that the volumetric mass transfer coefficient in such devices is much more than other conventional absorption columns [23]; however, the experimental investigations of CO_2 absorption in microchannels are complex and costly. Hence, computational fluid dynamics (CFD) can be applied to investigate the performance of solvents. By utilizing CFD, the novel and efficient type of micro-structured systems can be designed and the effect of various parameters can be studied more easily [24, 25]. Dong et al. simulated CO_2 absorption in a microchannel by MEA and NaOH solvents and compared the volumetric coefficient of chemical and physical absorptions of CO_2 [26]. They have found that the chemical absorption rate is 3 to 10 times more than physical absorption. In another CFD simulation of CO_2 absorption in microchannels, it is found that the mass transfer rate was enhanced by increasing the solvent concentration, liquid and gas superficial velocity, and operating temperature [27].

In general, applying the ionic liquids and nanoparticles as novel and efficient solvents in the absorption processes can improve the mass transfer rate in the system. Besides, microchannels as phase contactor are capable to increase the interfacial area and the mass transfer coefficient. In this research, a novel solvent is proposed for the first time for CO_2 capture by mixing of the aqueous solution of MEA as the base solution, and $[Bmim]BF_4$ ionic liquid and TiO_2 nanoparticles as chemical additives. Then, the flow hydrodynamics, mass transfer characteristics, and CO_2 absorption performance of the novel solvent are investigated in a microchannel by CFD technique. Besides, the effect of operating parameters such as gas to liquid velocity ratio and ionic liquid and nanoparticle weight fractions have been investigated.

2 Absorption and Reaction Mechanisms

The zwitterion mechanism which is introduced by Dankwerts explains the reaction of CO_2 with primary and secondary alkanolamines [28] Generally, unstable zwitterion molecules are formed when CO_2 reacts with MEA, and any bases can instantaneously neutralize the zwitterions with the following mechanism:

$$CO_2 + R_1R_2NH \underset{k_{-2}}{\overset{k_{2,MEA}}{\rightleftharpoons}} R_1R_2NH^+COO^- \tag{1}$$

$$R_1R_2NH^+COO^- + B_i \xrightarrow{k_{B_i}} R_1R_2NCOO^- + B_iH^+ \tag{2}$$

Although the dissolution of CO_2 into pure ILs is a physical phenomenon and no chemical reaction occurs, the ionic liquids can be hydrolyzed when dissolved in water [29]. The mechanism of CO_2 reaction with MEA and $[Bmim]BF_4$ is complex, since ILs may take an extra proton. Therefore, the reaction mechanism can be described as follows[30]:

$$R_1R_2NH^+COO^- + R_1R_2NH \xrightarrow{k_{B_{MEA}}} R_1R_2NCOO^- + R_1R_2NH^+ \tag{3}$$

$$R_1R_2NH^+COO^- + IL \xrightarrow{k_{B_{IL}}} R_1R_2NCOO^- + ILH^+ \tag{4}$$

$$IL + R_1R_2NH_2^+ \xrightarrow{k_{B_{IL}}} R_1R_2NH + ILH^+ \tag{5}$$

The overall rate of the CO_2 absorption can be explained as follows:

$$r = k_{ov}C_{CO_2} = \left(k_{MEA}C_{MEA} + k_{IL}C_{IL}\right)C_{CO_2}, \tag{6}$$

where k and C are the reaction rate constant and concentration, respectively. By using the enhancement factor, the concentration of CO_2 in the liquid bulk can be replaced by that of the interface, which is found from gas partial pressure in the bubbles divided by Henry's constant.

$$R_{CO_2} = Ek_L aC_{CO_2} = \frac{Ek_L aP_{CO_2}}{H}, \tag{7}$$

where R is the total mass transfer rate, E is the enhancement factor, k_L represents the liquid side mass transfer coefficient, a shows interfacial area, and H designates the Henry's constant. The enhancement factor can be expressed as follows:

$$E = \sqrt{1 + \frac{D_{CO_2}k_{ov}}{k_L^2}} \tag{8}$$

where D is the diffusion coefficient. The liquid side mass transfer coefficient can be calculated as [22]:

$$k_L = 2\sqrt{\frac{D_{CO_2}}{\pi\tau_c}} \tag{9}$$

where τ_c is residence time. Based on the presented data in the literature, the reaction rate is not affected by nanoparticles in CO_2 absorption process and only the diffusion coefficient and Henry's constant changes, which leads to better performance of the resulted solvent [31]. To calculate the diffusivity of CO_2 in the nanofluid, the following equation is used [32]:

$$D_{eff} = 1 + 1332.49(1 + \varphi Re)^{-2100.81}Sc^{-1.52533} \tag{10}$$

where φ is the mass fraction of the nanoparticle in the solution. Re and Sc are the Reynolds and Schmidt numbers of the nanofluids calculated by:

$$Re = \frac{2K_B T\rho_p}{\pi\mu^2 d_p}, \tag{11}$$

$$Sc = \frac{\mu_{\mathrm{nf}}}{\rho_{\mathrm{nf}} D_{\mathrm{CO_2}}}, \tag{12}$$

The viscosity and density of nanofluid can be calculated by [33]:

$$\mu_{\mathrm{nf}} = (1-\varphi)^{-2.5}\mu_{\mathrm{base}} \tag{13}$$

$$\rho_{\mathrm{nf}} = \varphi\rho_{\mathrm{p}} + (1-\varphi)\rho_{\mathrm{base}} \tag{14}$$

Henry's constant of nanofluids is estimated by applying the solubility enhancement factor to the solubility of the base fluid [11].

3 Simulation Procedure

To investigate the performance of CO_2 absorption in the microchannels, the COMSOL multiphase software is used [34]. The simulation approach consists of estimation of spatial flow velocity by laminar flow module, identifying the liquid and gas boundaries by two-phase flow model, and calculation of CO_2 concentration by mass transfer module.

3.1 Microchannel Geometry

Figure 1 shows the circular T-junction microchannel with 5 mm length and 250 μm diameter designed for CO_2 capture process in the current research. The microchannel consists of a horizontal section that is joined exactly to the middle of the vertical channel. The gas and liquid streams are fed from the top and bottom of the vertical channel,

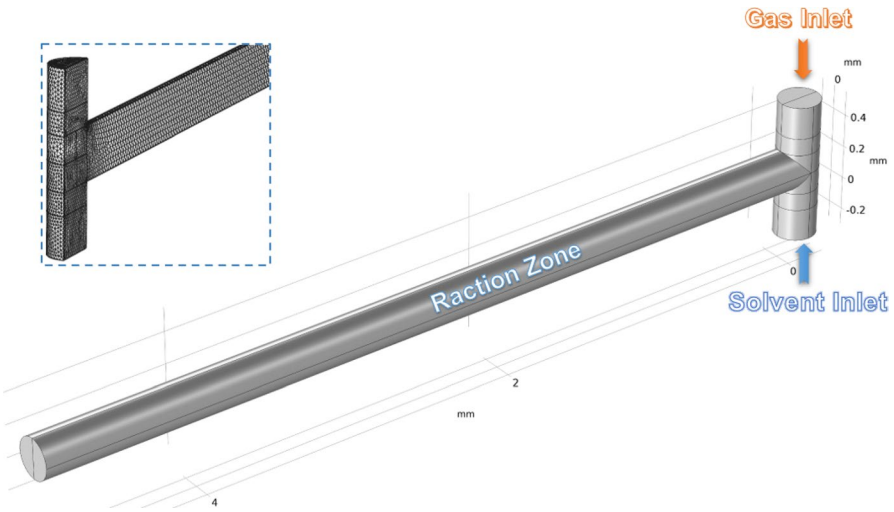

Fig. 1 T-shaped microchannel geometry and tetrahedral mesh distribution

respectively. To form bubbles, the liquid and gas streams contact at the junction point and flow through the main channel with. The tetrahedral mesh distribution is applied on the microchannel and symmetric boundary condition is considered at depth. For applying the appropriate mesh structure, the elements near the boundaries are supposed to be smaller, particularly in the junction point. As shown in the top section of Fig. 1, the geometry of the microchannel is divided into various sections to control mesh growth size and distribution.

3.2 Flow Model

3.2.1 Laminar Flow Model

The mass continuity and Navier–Stokes equations are applied to estimate the velocity profile and fluid hydrodynamics as follows:

$$\frac{\partial \rho}{\partial t} + \nabla \cdot (\rho \mathbf{u}) = 0 \tag{15}$$

$$\rho \frac{\partial \mathbf{u}}{\partial t} + \rho(\mathbf{u} \cdot \nabla)\mathbf{u} = \nabla.\left[-p\mathbf{I} + \tau_f\right] + \mathbf{F}, \tag{16}$$

where $\mathbf{u}$ is velocity vector, $\mathbf{F}$ is volume force vector, and τ_f indicates viscous stress tensor [35]. It has been assumed that the flow regime is laminar which leads to elimination of turbulence terms at the Navier–Stokes equations.

3.2.2 Two-Phase Flow Model

The dynamic transport equation is applied to evaluate the phase distribution in the designed microchannel [36]. This equation is explained as follows:

$$\frac{\partial \phi}{\partial t} + \mathbf{u}\nabla\phi = \gamma \nabla \left(\varepsilon \nabla \phi - \phi(1-\phi)\frac{\nabla \phi}{|\nabla \phi|} \right), \tag{17}$$

where ϕ is the volume fraction, γ is initialization parameter, and ε is interface controlling parameter whose value is equal to the maximum mesh size in which the interface passes through.

3.2.3 Flow Boundary Conditions

Before contacting the gas and liquid streams at the junction point, it is assumed that both streams are in the single-phase condition. In addition, the wetted wall boundary condition is applied to prevent any mass penetration across the wall.

3.3 Mass Transfer Model

By considering convection and diffusion mechanisms, the mass conservation equation across the microchannel can be written as follows:

$$\frac{\partial C_{CO_2}}{\partial t} + \nabla.\left(D_{CO_2}\nabla C_{CO_2}\right) + \mathbf{u}\cdot\nabla C_{CO_2} = R_{CO_2} \tag{18}$$

In the considered model, the bubble size change is neglected due to low CO_2 in the gas stream [37]. Since the molar ratio of inlet CO_2 to solvent is low and CO_2 reacts with MEA molecules chemically, the concentration of CO_2 in the liquid phase is negligible. In addition, the gradient of normal concentration for both phases has been assumed to be zero which means free outward flow to the atmosphere. To compare the performance of solvents at different additive fractions, the purification fraction defined as the relative amount of absorbed CO_2 is expressed as follows:

$$\eta = \frac{C^{in}_{CO_2} - C^{out}_{CO_2}}{C^{in}_{CO_2}} \times 100\,\% \tag{19}$$

4 Results and Discussions

In this section, the simulation results of CO_2 absorption in the designed microchannel are presented at ionic liquid fraction 0 % to 10 % and nanoparticle fraction 0 % to 0.1 %. The applied solvent contains 3% MEA as the base fluid. The CO_2 mole fraction in the inlet gas mixture and inlet liquid velocity is set to be 0.1 $cm{\cdot}s^{-1}$ and 3 $cm{\cdot}s^{-1}$, respectively. The simulations are conducted on a high-speed computer with 32 GB RAM and an Intel Core i7 6850 K processor running at 3.6 GH. Table 1 provides the properties of pure materials employed in the current study and Table 2 shows the calculated properties of NEILs by models and available experimental data in the literature. It can be found that addition of 10% IL to MEA increases the density, viscosity, and diffusivity up to 1.6 %, 16.3 %, and 7.88 %, respectively. Although the addition of 0.05 % nanoparticle to the solution containing 3 % MEA

Table 1 Pure materials properties [32, 40, 41]

Name	Formula	Phase	M_w ($g{\cdot}mol^{-1}$)	ρ ($kg{\cdot}m^{-3}$)	μ ($mPa{\cdot}s^{-1}$)
Carbon dioxide	CO_2	Gas	44.01	1.98	0.015
Nitrogen	N_2	Gas	28.01	1.25	0.018
Water	H_2O	Liquid	18.02	995.65	0.797
MEA	C_2H_7NO	Liquid	61.08	1.01	15.137
[Bmim]BF_4	$C_8H_{15}BF_4N_2$	Liquid	226.02	1.20	72.510
Titanium dioxide	TiO_2	Solid	79.87	3800	–

Table 2 MEA + IL solutions characteristics at 303.15 K [42]

w_{NP} (%)	w_{MEA}	w_{IL}	ρ_{mix} (kg·m^{-3})	μ_{mix} (mPa·s^{-1})	D_{mix} (10^9 m^2·s^{-1})	H_{mix} (Pa·m^3·mol^{-1})	k_{ov} (s^{-1})
0	3	0	998.9	0.986	2.03	3373.51	1403.18
0	3	10	1015.4	1.147	2.19	2898.43	1426.49
0.05	3	10	1015.8	1.148	2.43	2531.38	1426.49

and 10 % [Bmim]BF_4 has a significant effect on the density and viscosity, it can enhance the diffusivity up to 10.9 % and reduce Henry's constant up to 12.6 %. Figure 2 shows the density and Henry's constant of proposed NEIL solvent versus nanoparticle weight fraction. It appears that the increasing TiO_2 nanoparticle weight fraction in the range 0 % to 10 % increases the density of the solvent continuously. In contrast, Henry's constant shows a parabolic behavior with a minimum as illustrated in Fig. 2b. According to the hydrodynamic effect theory, nanoparticles can enhance the specific interfacial area via covering the surface of bubbles and preventing the bubble coalescence, which leads to smaller bubbles [38]. Another probability is the collision of nanoparticles and inducing local turbulence which result in refreshing the gas–liquid boundary layer via mixing it into the bulk liquid [39]. The aforementioned mechanisms can improve the solubility of CO_2 into the solution which affects Henry's constant.

4.1 Channel Hydrodynamics

Figure 3 indicates the velocity profile and streamlines at various inlet gas velocities in the designed microchannel. It appears that the fluid velocity increases along the radial direction and the maximum velocity appears at the centerline of the channel. In addition, the inlet gas bubbles are compressed by the liquid stream at the junction point and a narrow passage is developed to flow gas stream. On the other hand, the liquid flow layers are also affected by the gas bubble entrance and streamlines compressed a bit. However, the effect of gas compression on the velocity enhancement is more important and the maximum velocity is developed at the junction point. In general, the mean fluid velocity at the horizontal part and the entrance of the microchannel are 15 cm·s^{-1} and 5 cm·s^{-1}, respectively, while the mean fluid velocity increases up to 30 cm·s^{-1} at the junction point of the microchannel. On the other hand, gas to liquid velocity ratio has a significant effect on the fluid velocity along the microchannel. Therefore, increasing the velocity ratio from 1.7 cm·s^{-1} to 3 cm·s^{-1} increases the maximum fluid velocity at the junction point up to two times.

4.2 Mass Transfer Characteristics

While the bubbles containing a mixture of CO_2 and N_2 flows along the microchannel, the CO_2 molecules absorb into the liquid solution and react with MEA and hydrolyzed [Bmim]BF_4 molecules. Generally, the residence time and solvent concentration have considerable effects on the amount of absorbed CO_2 in the liquid.

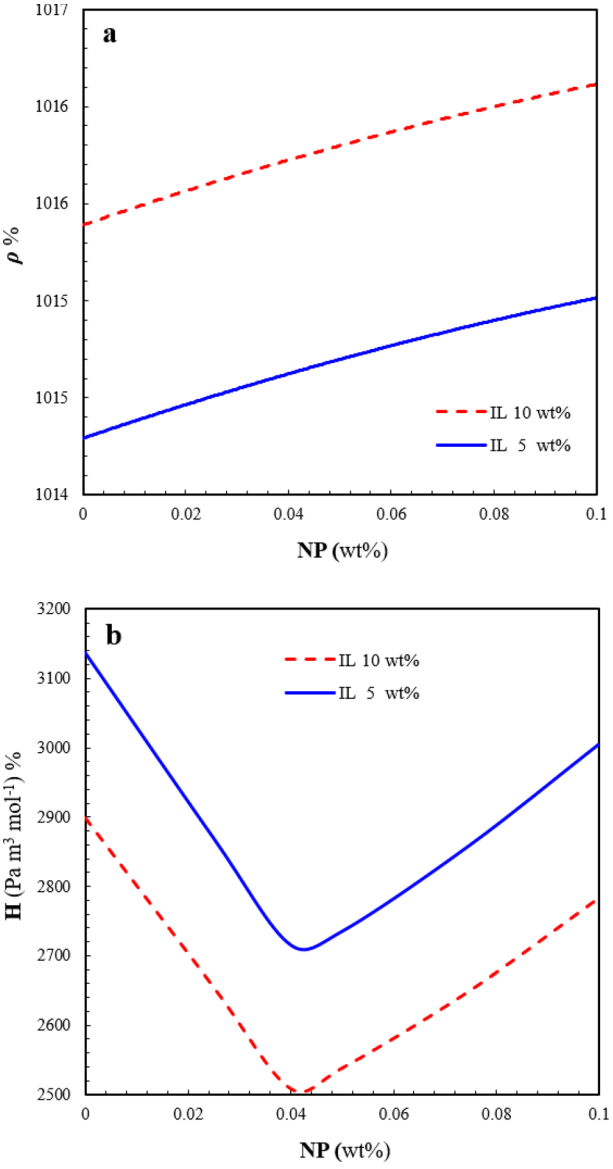

Fig. 2 Thermophysical properties of utilized NEILs: (a) density and (b) Henry's constant

The residence time, which is controlled by the channel length and fluid flow rates, has a crucial role and limits the exposure of the two phases. Increasing residence time shifts absorption toward the equilibrium condition. Based on the kinetic of gas absorption in liquid, applying high concentration solvents increases the rate of CO_2 absorption. Figure 4 shows the CO_2 mole fraction along the channel at different [Bmim]BF_4 ionic liquid and TiO_2 nanoparticle weight fractions. Due to the

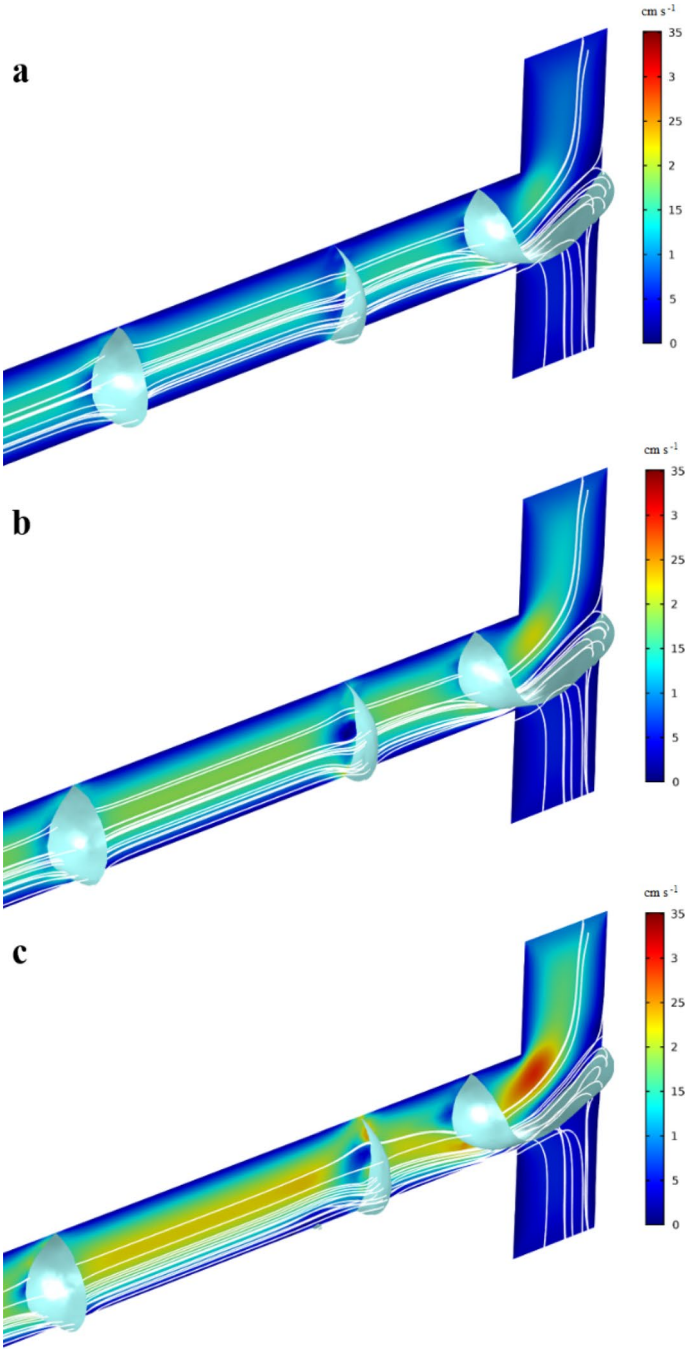

Fig. 3 Velocity magnitude and stream lines for different inlet gas velocities at IL 5 wt % and NP 4 wt %: (a) $u_{GL}=1.7$ cm·s^{-1}, (b) $u_{GL}=2.3$ cm·s^{-1}, and (c) $u_{GL}=3.0$ cm·s^{-1}

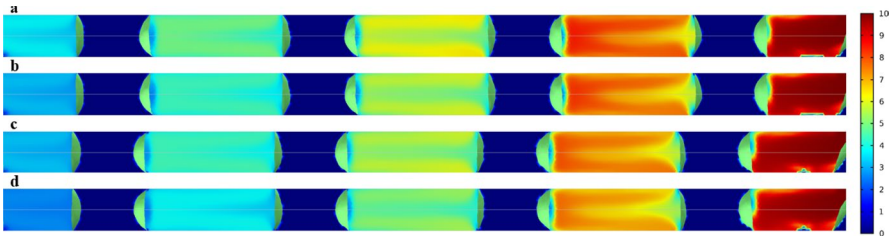

Fig. 4 CO_2 mole fraction variation along the channel at $u_{GL}=2.3$ cm·s^{-1}: (a) IL 0 wt % and NP 0 wt %, (b) IL 0 wt % and NP 0.04 wt %, (c) IL 10 wt % and NP 0 wt %, and (d) IL 10 wt % and NP 0.04 wt %

solubility of CO_2 in the solvent, as bubbles move along the microchannel, the concentration of CO_2 in the gas phase decreases. It appears that the addition of nanoparticles into the base fluid enhances CO_2 solubility in the liquid phase and CO_2 molecules are absorbed more rapidly to the liquid phase. On the other hand, it can be found that the addition of [Bmim]BF_4 ionic liquid into the base solution increases CO_2 solubility. Hence, aqueous mixture of [Bmim]BF_4 ionic liquid and MEA by TiO_2 nanoparticle results in maximum absorption performance.

Figure 5 shows the CO_2 mole fraction along the designed microchannel at different gas to liquid velocities ratios. It appears increasing the gas flow rate increases the length of formed bubbles and decreases the bubble resident time in the microchannel. In general, increasing gas to liquid velocity decreases gas residence time in the microchannel and results in a higher CO_2 concentration in the outgoing bubbles. It must be considered that increasing or decreasing the gas flow rates can change the flow pattern from Taylor to annular or bubbly, which decreases the mass transfer coefficient across the microchannel [32].

Figure 6 shows the purification fraction at different gas to liquid velocities ratios and [Bmim]BF_4 and TiO_2 weight fractions. It appears that increasing the TiO_2 weight fraction in the solvent enhances the purification fraction up to a maximum value and after that, the purification decreases gradually. When the concentration of nanoparticles in the solvent is low, nanoparticles move rapidly in the fluid and enhance the mass transfer coefficient in the system. On the other hand, since the volumetric flow rate of the solvent has been fixed in all cases, increasing nanoparticle weight fraction decreases MEA and [Bmim]BF_4 content in the applied solvent and

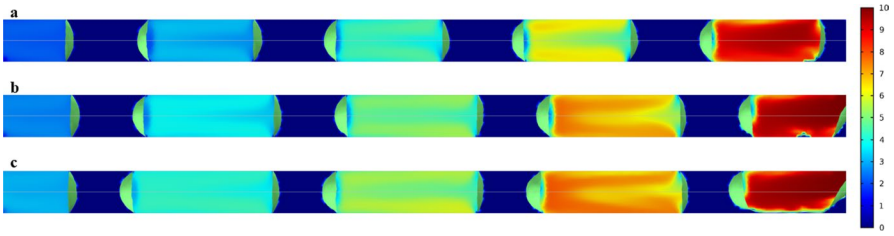

Fig. 5 CO_2 mole fraction variation through the channel for different inlet gas velocities IL 10 wt % and NP 0.04 wt %: (a) $u_{GL}=1.7$ cm·s^{-1}, (b) $u_{GL}=2.3$ cm·s^{-1}, and (c) $u_{GL}=3.0$ cm·s^{-1}

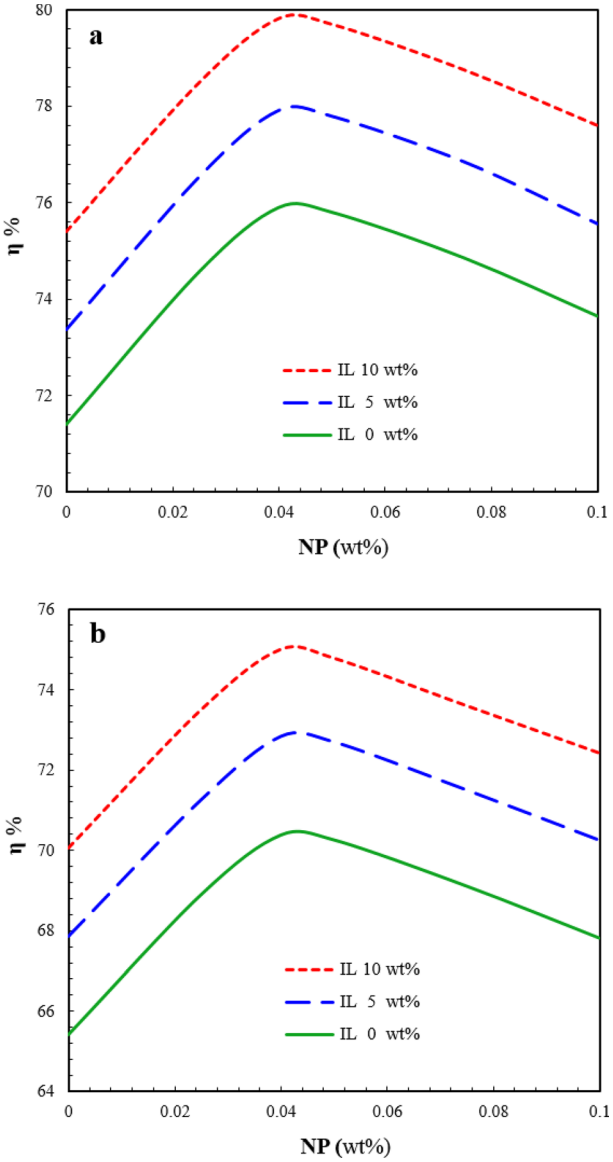

Fig. 6 Purification fraction for different ionic liquid weight fractions: (a) $u_{GL}=1.7$ cm·s^{-1}, (b) $u_{GL}=2.3$ cm·s^{-1}, and (c) $u_{GL}=3.0$ cm·s^{-1}

could result in lower CO_2 absorption. From a practical viewpoint, increasing nanoparticle concentration can hinder the interaction of particles which leads to precipitation and agglomeration of nanoparticles in the fluid [11]. It concludes that there is an optimal value for nanoparticle concentration in the solvent to achieve a maximum purification ratio. Based on the simulation results, decreasing gas to liquid velocity

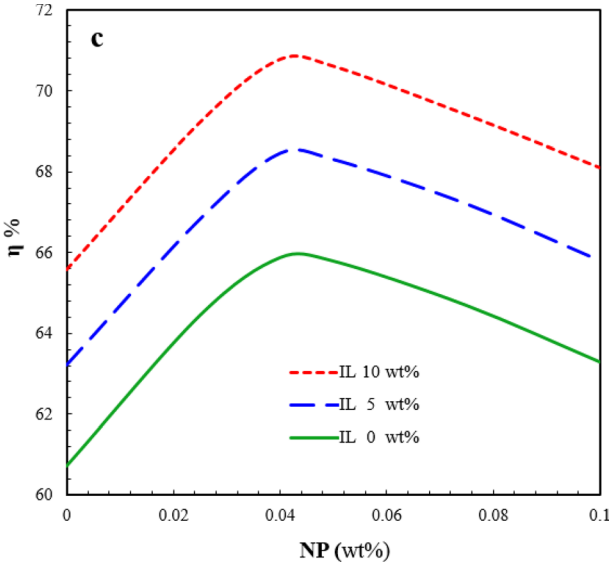

Fig. 6 (continued)

enhances the purification fraction due to increasing gas residence time in the microchannel. Increasing the [Bmim]BF_4 weight fraction from 0 % to 10 % at the gas to liquid velocity 1.7 m·s^{-1} and the nanoparticle weight fraction 0.04 % changes the purification ratio from 78.49 % to 79.62 %, while increasing the velocity ratio from 1.7 m·s^{-1} to 2.3 cm·s^{-1} decreases the purification fraction to 70.54 %.

Figure 7 illustrates the effect of gas to liquid velocity on the purification fraction. Variation of gas to liquid gas velocity changes the gas and liquid hold up in the process and it affects the contact time. As mentioned previously, increasing the gas to liquid velocity reduces the resident time of gas bubbles in the microchannel. Therefore, the mass transfer coefficient decreases and the CO_2 transfer from bubbles to the liquid phase is reduced considerably. It is shown that decreasing the gas to liquid velocity from 3 cm·s^{-1} to 1.7 cm·s^{-1} improves the purification fraction from 70.77 % to 79.82 % in the sample that contains 10 % ionic liquid and decreases the CO_2 mole fraction at the outgoing bubbles from 2.92 % and 2.02 %. Since decreasing the flow rate in the microchannel highly affects the process economy, it is suggested to maintain the gas velocity at the maximum level in which the Taylor flow regime is still valid.

5 Conclusions

In this research, a detailed model including Navier–Stokes and continuity equations combined with mass transfer and two-phase flow equation was developed to simulate CO_2 absorption by a novel nanofluid in a T-shaped microchannel. The proposed nanofluid solvent included MEA as the base fluid, and [Bmim]BF_4 ionic liquid and

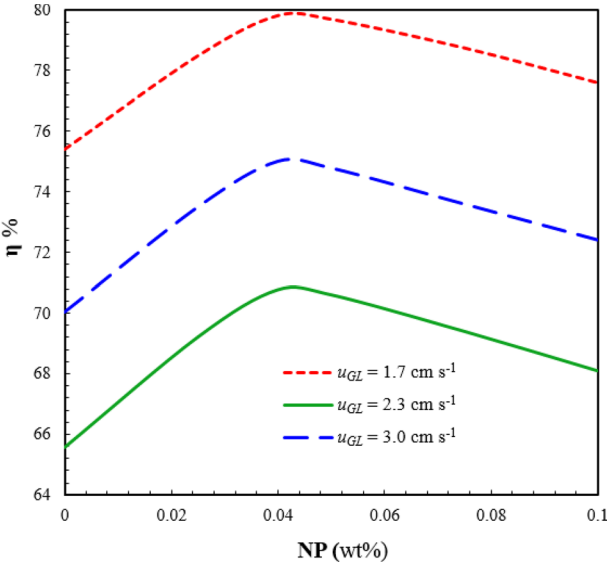

Fig. 7 Purification fraction for different velocity ratios for IL 10 wt % and NP 0.04 wt %

TiO_2 nanoparticles as chemical additives. The COMSOL Multiphysics software was utilized to simulate the absorption process by applying tetrahedral mesh distribution on the designed geometry. According to the simulation results, the maximum gas velocity was developed at the junction point of the microchannel due to the narrow passage for the flow stream. Although increasing [Bmim]BF_4 concentration in the considered solvent increased the purification fraction, increasing the TiO_2 weight fraction in the solvent enhanced the purification fraction up to a maximum value, and after that, the purification fraction decreased gradually. On the other hand, increasing the inlet gas to liquid velocities ratio in the microchannel decreased the gas residence time in the microchannel and reduced the CO_2 loading. Based on the simulation results, the solvent containing 10 % [Bmim]BF_4, 3 % MEA, and 0.04 % TiO_2 presented the maximum purification fraction of 79.62 %.

References

1. S. Keskin, D. Kayrak-Talay, U. Akman, Ö. Hortaçsu, J Supercrit Fluids **43**, 150 (2007)
2. A.-L. Revelli, F. Mutelet, J.-N. Jaubert, J. Phys. Chem. B **114**, 12908 (2010)
3. J. Zhang, J. Sun, X. Zhang, Y. Zhao, S. Zhang, Greenh. Gases Sci. Technol. **1**, 142 (2011)
4. M.E. Boot-Handford, J.C. Abanades, E.J. Anthony, M.J. Blunt, S. Brandani, N. Mac Dowell, J.R. Fernández, M.-C. Ferrari, R. Gross, J.P. Hallett, Energy Environ. Sci. **7**, 130 (2014)
5. G. Cevasco, C. Chiappe, Green Chem. **16**(5), 2375 (2014)
6. R. Giernoth, Angew. Chem. Int. Ed. **49**, 2834 (2010)
7. Z.-Z. Yang, Y.-N. Zhao, L.-N. He, RSC Adv. **1**, 545 (2011)
8. M. Pishnamazi, A.T. Nakhjiri, A.S. Taleghani, A. Marjani, A. Heydarinasab, S. Shirazian, J. Mol. Liq. **314**, 113635 (2020)
9. M. Mofarahi, M.A. Makarem, P. Jowkar, B. Jafarian, Heat Transf. Asian Res. **45**, 358 (2016)

10. T. Wang, W. Yu, F. Liu, M. Fang, M. Farooq, Z. Luo, Ind. Eng. Chem. Res. **55**, 7830 (2016)
11. J.-Z. Jiang, L. Liu, B.-M. Sun, Int. J. Greenh. Gas Control **60**, 51 (2017)
12. A.A. Minea, Int. J. Thermophys. **41**, 1 (2020)
13. A. Joseph, P.R. Nair, S. Mathew, Int. J. Thermophys. **41**, 1 (2020)
14. L.-L. Zhang, J.-X. Wang, Y. Xiang, X.-F. Zeng, J.-F. Chen, Ind. Eng. Chem. Res. **50**, 6957 (2011)
15. M.R. Kiani, M.A. Makarem, M. Farsi, M.R. Rahimpour, *Advances in Carbon Capture* (Elsevier, Oxford, 2020), pp. 151–170
16. J.-C. Charpentier, *Advances in Chemical Engineering* (Elsevier, New York, 1981), pp. 1–133
17. W. Ehrfeld, V. Hessel, H. Lowe, *Microreactors—New Technology for Modern Chemistry* (Wiley-VCH, New York, 2000).
18. K.F. Jensen, Chem. Eng. Sci. **56**, 293 (2001)
19. G. Kolb, V. Hessel, Chem. Eng. J. **98**, 1 (2004)
20. M.W. Losey, M.A. Schmidt, K.F. Jensen, Ind. Eng. Chem. Res. **40**, 2555 (2001)
21. J. Yue, L. Luo, Y. Gonthier, G. Chen, Q. Yuan, Chem. Eng. Sci. **63**, 4189 (2008)
22. M. Makarem, M. Farsi, M. Rahimpour, Int. J. Hydrog. Energy (2020). https://doi.org/10.1016/j.ijhydene.2020.07.22
23. R. Guo, C. Zhu, Y. Yin, T. Fu, Y. Ma, J. Ind. Eng. Chem. **75**, 194 (2019)
24. V.K. Bodla, R. Seerup, U. Krühne, J.M. Woodley, K.V. Gernaey, Chem. Eng. Technol. **36**, 1017 (2013)
25. N. Harries, J. Burns, D.A. Barrow, C. Ramshaw, Int. J. Heat Mass Transf. **46**, 3313 (2003)
26. R. Dong, D. Chu, Q, Sun, Z, Jin, (2020) The Canadian J. Chem. Eng. **98**, 2648 (2020). https://doi.org/10.1002/cjce.23781
27. S. Firuzi, R. Sadeghi, Microfluid. Nanofluid. **22**, 109 (2018)
28. P. Danckwerts, Chem. Eng. Sci. **34**, 443 (1979)
29. D. Camper, P. Scovazzo, C. Koval, R. Noble, Ind. Eng. Chem. Res. **43**, 3049 (2004)
30. B.-H. Lu, J.-J. Jin, L. Zhang, W. Li, Int. J. Greenh. Gas Control **11**, 152 (2012)
31. B. Lu, X. Wang, Y. Xia, N. Liu, S. Li, W. Li, Energy Fuels **27**, 6002 (2013)
32. P. Dehghan, A. Azari, R. Azin, J. Environ. Chem. Eng. **8**, 103598 (2020)
33. M.A. Makarem, A. Bakhtyari, M.R. Rahimpour, Heat Transf. Asian Res. **47**, 347 (2018)
34. M.B. Turgay, A.G. Yazıcıoğlu, Numer. Heat Transf. Part A Appl. **73**, 332 (2018)
35. G.G. Stokes, Trans. Camb. Philos. Soc. **IX**, 8 (1880)
36. COMSOL AB, www.comsol.com. Stockholm, Sweden
37. H. Ganapathy, E. Al-Hajri, M. Ohadi, Chem. Eng. Sci. **101**, 69 (2013)
38. V. Linek, M. Kordač, M. Soni, Chem. Eng. Sci. **63**, 5120 (2008)
39. K.C. Ruthiya, J. van der Schaaf, B.F. Kuster, J.C. Schouten, Int. J. Chem. Reactor Eng. **4**, A13 (2006)
40. T.G. Amundsen, L.E. Øi, D.A. Eimer, J. Chem. Eng. Data **54**, 3096 (2009)
41. J. Li, H. Zhu, C. Peng, H. Liu, Chin. J. Chem. Eng. **27**, 2994 (2019)
42. Y. Yin, T. Fu, C. Zhu, R. Guo, Y. Ma, H. Li, Sep. Purif. Technol. **210**, 541 (2019)